Lawrence Berkeley National Laboratory
Recent Work

Title
Effect of Anisotropic Confinement on Electronic Structure and Dynamics of Band Edge Excitons in Inorganic Perovskite Nanowires.

Permalink
https://escholarship.org/uc/item/3wp3q21w

Journal
The journal of physical chemistry. A, 124(9)

ISSN
1089-5639

Authors
Folie, Brendan D
Tan, Jenna A
Huang, Jianmei
et al.

Publication Date
2020-03-01

DOI
10.1021/acs.jpca.9b11981

Peer reviewed

Effect of Anisotropic Confinement on Electronic Structure and Dynamics of Band Edge Excitons in Inorganic Perovskite Nanowires

Brendan D. Folie[1], Jenna A. Tan[2], Jianmei Huang[2], Peter C. Sercel, Milan Delor[2], Minliang Lai[2], John L. Lyons**, Noam Bernstein**, Alexander L. Efros**, Peidong Yang[2,3,5,6], Naomi S. Ginsberg[1,2,4,5,6†]*

[1]Department of Physics, [2]Department of Chemistry, and [3]Department of Materials Science and Engineering, University of California, Berkeley, California 94720, United States

[4]Molecular Biophysics and Integrated Bioimaging Division and [5]Materials Sciences Division, Lawrence Berkeley National Laboratory, Berkeley, California 94720, United States

[6]Kavli Energy NanoSciences Institute, Berkeley, California 94720, USA.

*Department of Applied Physics and Materials Science, California Institute of Technology, Pasadena CA 91125
** Center for Computational Material Science, Naval Research Laboratory, Washington DC 20375, USA

[†]Corresponding author email address: nsginsberg@berkeley.edu

Abstract:
Inorganic lead halide perovskite nanostructures show promise as the active layers in photovoltaics, light emitting diodes, and other optoelectronic devices. They are robust in the presence of oxygen and water, and the electronic structure and dynamics of these nanostructures can be tuned through quantum confinement. Here we create aligned bundles of $CsPbBr_3$ nanowires with widths resulting in quantum confinement of the electronic wavefunctions and subject them to ultrafast microscopy. We directly image rapid one-dimensional exciton diffusion along the nanowires, and we measure an exciton trap density of roughly one per nanowire. Using transient absorption microscopy, we observe a polarization-dependent splitting of the band edge exciton line, and from the polarized fluorescence of nanowires in solution we determine that the exciton transition dipole moments are anisotropic in strength. Our observations are consistent with a model in which splitting is driven by shape anisotropy in conjunction with long-range exchange.

Introduction:

Inorganic lead-halide perovskite materials, $APbX_3$, where A is an inorganic cation and X is a halogen or combination of halogens, are currently being intensively studied both for their interesting physical properties and for their promise as the active material in optoelectronic devices. Photovoltaics are the marquee example of a perovskite device, with high charge carrier mobilities, strong optical absorption, and efficient photoluminescence (PL)—all correlated to efficiencies above 12%.[1,2] These same properties have been used to produce lasers with low lasing thresholds and high quality factors,[3,4] as well as sensitive photodetectors[5,6] and scintillators.[7] One advantage of an inorganic cation is that the resulting material is relatively robust, even in the presence of oxygen and water[2,4,8] and, with encapsulation, can be made stable over an extended period of illumination.[9]

Many of the above applications involve nanostructures, in part because size offers a route to tune properties,[10-13] and also because novel behaviors can emerge when the material dimensions become comparable to the exciton Bohr radius, which is typically a few nanometers.[5] For this reason one prototypical inorganic halide perovskite, $CsPbBr_3$, has been extensively studied in nanocube form. For example, it has been found that optical emission occurs with sub-ns lifetimes with high quantum efficiency in nanocubes of $CsPbBr_3$,[10] which has been ascribed to an inversion of the level order of the bright and dark fine structure levels caused by the Rashba effect. Geometry also plays an important role, as confinement makes biexciton interactions more prevalent[14,15] and the presence of surface states can affect carrier trapping.[16] Despite this work on $CsPbBr_3$ nanocubes, much less is known about the properties of nanoplatelets or nanowires, in which confinement is limited to one or two dimensions. Yet they are worthy of separate study – nanoplatelets and nanowires can produce novel assemblies,[12,17] modify the electronic states in unique ways,[18] change the primary exciton decay mechanism,[19] and lead to new behaviors such as exciton dissociation at edge states,[20] or polarization-dependent optical interactions.[6,21]

3

Here we investigate the anisotropic transport properties of and polarization-dependent optical interactions with $CsPbBr_3$ nanowires with lateral widths of 10 nm. We do so by producing nanowire bundles – many monodisperse nanowires aligned parallel to one another yet essentially non-interacting. We image carrier diffusion within a single bundle using a pump-probe elastic scattering microscopy, stroboSCAT (stroboscopic interferometric scattering microscopy).[22] We find rapid, highly anisotropic diffusion through an environment with extremely low trap densities. Separately, we measure the polarization-resolved ultrafast electronic dynamics with transient absorption microscopy. We find that the dynamics are similar to those of bulk $CsPbBr_3$ but that the band-edge transition energy depends on the polarization of the incident light relative to the nanowire axis. Finally, we use fluorescence anisotropy measurements in solution to infer a corresponding anisotropy in the transition dipole moment strengths. The polarization-dependent splitting of the band edge exciton is consistent with splitting due to long-range exchange in conjunction with the shape anisotropy of the nanowire[23,24] while density functional theory (DFT) calculations indicate that crystal field effects cannot explain the observed polarization dependent splitting. The magnitude of the observed splitting suggests that two-dimensional confinement of the exciton in nanowires, in conjunction with dielectric confinement effects associated with the difference in the dielectric constant of the nanowire and the surrounding medium,[25] causes enhancement of the exciton binding energy relative to bulk excitons, with a concomitant increase in the long-range exchange splitting energy.

Experimental Details:

Materials:
Cs_2CO_3 (99.9%), CsBr (99.999%), $PbBr_2$ (99.999%, Alfa Aesar), PbI_2 (99.999%), 1-octadecene (ODE, 90%), oleic acid (OlAc, 90%), oleylamine (OlAm, 70%), Hexanoic acid (HexAc, ≥99.5%), octylamine (OctAm 99.5%), Toluene (99.9%, Fisher Scientific), Cyclohexane (99.5%), Dimethylformamide (DMF), Methanol (anhydrous, 99.8%), Isopropanol (anhydrous). All chemicals were used as received without further purification. All chemicals were purchased from Sigma-Aldrich unless otherwise noted.

Cs-oleate solution was prepared by loading 0.2 g Cs_2CO_3 and 0.7 mL OlAc into a 3-neck flask along with 7.5 mL ODE, degassing for 40 mins at 120 ºC under vacuum, and then heating under N_2 to 150 ºC until all Cs_2CO_3 reacted with OlAc.

Nanowire Synthesis and Deposition:
10 nm thick nanowires were prepared following Zhang et. al.[26] 5 mL ODE and 0.2 mmol $PbBr_2$ were loaded into a 3-neck flask and degassed under vacuum for 30 mins at 120 °C. 0.8 mL dried OctAm and 0.8 mL dried OlAm were injected at 120 °C under N_2. The temperature was raised to 135 °C and the solution was stirred for 20 mins. 0.7 mL of as-prepared Cs-oleate solution was swiftly injected into the opaque white solution. After 50 mins, the reaction mixture was cooled by an ice-water bath. The NWs were isolated by centrifugation at 6000 rpm for 5 mins and washed once with toluene. The

obtained precipitated NWs were re-dispersed in toluene or cyclohexane for further use. Dispersing in toluene results in nanowire bundles, whereas cyclohexane helps to obtain isolated nanowires.

Large (hundreds of nm thick) $CsPbBr_3$ nanowires were prepared following Eaton et. al.[3] 460 mg PbI_2 was dissolved in 1 mL anhydrous DMF and stirred at 70 °C overnight before further use. The PbI_2 solution was spun onto a PEDOT: PSS-coated glass substrates (Solarmer) at 1000~3000 rpm for 120 s, then annealed at 100 °C for 15 min. The PbI_2 film was carefully submerged into a glass vial containing a solution of 8 mg/mL CsBr in methanol, with the PbI_2 side facing up. The capped reaction vial was heated at 50 °C for 12 h, and the substrate was removed after cooling for some time. Then the substrate was washed twice in isopropanol (each time for 30 s). The sample was then dried by heating to 50 °C for 5 min.

Nanowire solutions were diluted and deposited by drop casting onto glass coverslips cleaned by sonication in acetone, isopropanol, and Millipore water. In order to speed evaporation of the droplet, the coverslip was placed in a petri dish on a hot plate heated to 60 °C. The petri dish was regularly picked up and tilted in order to spread the nanowires around on the coverslip. Individual bundles were located by inspection.

Characterization:

Transmission electron microscopy (TEM) images of nanowires were taken on a Hitachi H7650 at an accelerating voltage of 120 kV.

Absorption measurements were done in an Agilent Cary 100 UV-Vis spectrophotometer. Fluorescence measurements were done in a PicoQuant FluoTime 300 fluorimeter, using PicoQuant pulsed diode lasers and a PDL 820 driver. The instrument response function of the system was less than 500 ps in duration. Emitted light was collected in a right-angle geometry, with the excitation and emission propagation directions perpendicular to each other in a horizontal plane. The diode laser was rotated to produce light polarized vertically or horizontally in the lab frame. The emitted light passed through a polarizer and a monochromator. Time-resolved fluorescence was measured with a TimeHarp 260 Time-Correlated Single Photon Counting Board.

For transient absorption (TA), an 80 MHz mode-locked Ti:sapphire Coherent Vitara oscillator was used to create a seed pulse, which fed a Coherent Legend-Elite regenerative amplifier. The output was split, with one line focused onto a CaF_2 plate to create the broadband probe. The other line was sent into a BBO crystal to produce 400 nm pump light, and into an optical parametric amplifier (Coherent OPerA Solo) to create 490 nm pump light. In ordinary TA the pump and probe were focused onto the sample with curved mirrors, the pump was spatially filtered, and the probe was detected with an Ocean Optics USB4000 spectrometer. In TA microscopy, the pump and probe were combined with a beam splitter and focused on the sample through an objective lens with a numerical aperture of 0.70. After re-collimating through a second objective lens after the sample, the pump was spectrally filtered and the probe was dispersed with a diffraction grating onto an Orion 2K Line Scan camera from Lightwise.

Local linear absorption measurements were done in the TA microscope, using lamp light from a monochromator. The light was sent through a polarizer and half-wave plate, then focused onto the sample and imaged on a camera. By recording the transmitted light intensity both through the sample and through a nearby spot on the coverslip, absent of sample, we measure the absorption as a function of wavelength and polarization.

StroboSCAT was done using pulsed diode lasers from PicoQuant: 440 nm (pump) and 640 nm (probe), synchronized with a PDL 828 "Sepai II" driver in a home built reflection-mode microscope. The pump laser was focused through an objective onto the sample, while the probe was focused onto the back focal plane of the objective, causing uniform illumination of the sample. The scattered probe light was interfered with a reflection off of the sample-substrate interface and imaged with a Pixelink PL-D752Mu-T camera.

Results and Discussion

In order to investigate the effect of two-dimensional confinement on $CsPbBr_3$, we synthesize monodisperse nanowires with widths of 10 nm.[27] Nanostructures of $CsPbBr_3$ typically adopt an orthorhombic[16,27-29] (shown in Figure 1a) or tetragonal[30] crystal structure, and are capped with ligands for stability. In toluene the nanowires self-assemble into bundles, illustrated in Figure 1b. A transmission electron microscopy (TEM) image of a 10 nm nanowire bundle is shown in Figure 1c. The nanowires are monodisperse and well-aligned with each other. Optical images of drop cast bundles are shown in Figure 1d. Note that individual bundles can be located and that the bundles can be up to several microns in width and tens of microns in length – larger than the optical spots used in transient absorption microscopy (indicated in Figure 1d).

Absorption and PL spectra of nanowire bundles in solution are shown in Figure 1e. PL measurements of several individual bundles are found to have identical fluorescence spectra (Figure S1), implying inter-bundle consistency. The time-resolved PL exhibits a multi-exponential decay (Figure S2). The exciton Bohr diameter of bulk $CsPbBr_3$ is roughly 7 nm,[31,32] meaning that 10 nm nanowires are in the weak confinement regime. This manifests as a slightly larger bandgap and bluer absorption, as can be seen by comparing against bulk $CsPbBr_3$ (see below). We conclude that bundled nanowires still experience the effects of quantum confinement.

We use stroboSCAT to image exciton diffusion along both the longitudinal and transverse axes of the nanowire bundles, which enables us to characterize the barriers to exciton transport. stroboSCAT employs interferometric scattering (iSCAT) as a probe, which uses the interference between light scattered off of the sample and its substrate in order to achieve exquisitely sensitive images. In stroboSCAT, a separate pump pulse is first focused onto the sample, and the resulting excited species appear in the iSCAT image due to their perturbation to the local polarizability. Controlling the time delay between the pump and the

iSCAT pulse allows us to track energy migration.[33] An iSCAT image of a nanowire bundle is shown in Figure 2a, and stroboSCAT snapshots at time delays of 0.0 ns, 0.4 ns, and 1.0 ns are shown in Figure 2b-d. The dark patch indicates increased polarizability due to the presence of excited species, and it can be seen to expand along the bundle as time advances. To quantify the extent of diffusion we plot profiles along the red dashed lines drawn in Figure 2b-d. These profiles, which show longitudinal diffusion, are shown in Figure 2e. The tails of the distribution broaden with time, indicating that exciton diffusion occurs. In order to track transverse diffusion we also excite along the side of a bundle and plot transverse profiles, shown in Figure S3. Transverse diffusion, which is indicative of inter-nanowire energy transfer, is seen to occur, although it is much slower than longitudinal diffusion.

By fitting the above stroboSCAT data to a model we are able to extract the intrinsic longitudinal diffusivity of $CsPbBr_3$ nanowires, as well as the inter-nanowire transverse diffusivity. The profiles in Figure 2e are fit to Gaussian functions in order to extract the mean squared displacement (MSD) of the excitons σ^2, where σ is the standard deviation of the Gaussian fit. The MSD as a function of pump-probe delay time is shown in Figure 2f. Ordinary diffusion would present a straight line from which we could extract the diffusivity, but that is clearly not the case here. We find that the data in Figure 2f fit well to an exponentially decaying effective diffusivity, $D(t)=D_0 e^{-t/\tau_d}$, where D_0 is the initial diffusivity and τ_d is the diffusion decay time. This leads to an exciton distribution that broadens as:

$$\sigma(t)^2=\sigma_0^2+2D_0\tau_d(1-e^{-t/\tau_d}), \qquad (1)$$

which is the red line of best fit plotted in Figure 2f. This is an unusual result. We first consider that the excitons diffuse through an energetically disordered landscape, which could lead to sub-diffusive behavior. However, that behavior would manifest as a power law,[34] $D(t)=D_0 t^{\alpha-1}$, and that functional form provides a poor fit to the data (Figure S4). In some works, an exponentially decaying diffusivity has been attributed to hot carrier cooling,[35] but that process occurs over a picosecond timescale,[36] and cannot explain the nanosecond-scale decay that we observe. We also consider that our observations could be an artifact of non-linear annihilation, which would cause the center of the distribution to decrease faster than the tails, providing the illusion of initially rapid diffusion. Varying the pump fluence, however, has no noticeable effect on τ_d, indicating that nonlinear exciton-exciton interactions cannot be responsible for the observed behavior.

Having ruled out several potential causes of the exponentially decaying diffusivity, we hypothesize that exciton traps limit exciton diffusion. These could be surface traps due to atomic defects or incomplete ligand coverage. We construct a model and use it to extract the intrinsic exciton diffusivity and the

7

trap density. The model consists of a population of mobile excitons, $p_m(x,t)$, and trapped excitons, $p_{tr}(x,t)$. The mobile excitons diffuse in one dimension with diffusivity D, while the trapped excitons are stationary. We use a spatially uniform trapping rate, k_{tr}, and both populations decay with rate k_{fl}. The equations for this model are:

$$\frac{\partial p_m}{\partial t} = D\frac{\partial^2 p_m}{\partial x^2} - k_{tr}p_m - k_{fl}p_m \quad \frac{\partial p_{tr}}{\partial t} = k_{tr}p_m - k_{fl}p_{tr}.$$

(2)

There are several simplifications in this model. First, although excitons are the dominant excited species, charge carriers are likely present as well, since the bulk exciton binding energy is only about 40 meV.[32] Also, the exciton decay is more complicated than a single rate constant, as seen in Figure S2, and we expect that trapping modifies the decay rate. Further study of the trapped exciton dynamics might provide insight into the traps' localization energy and allow for a more sophisticated model. Finally, trapping is not spatially uniform, although given that the distance between traps is likely too small to be spatially resolved, this is a good approximation. More importantly trapping is not temporally uniform – as traps fill, we might expect the rate to decrease. Nevertheless, we find that the model in Equation 2 fits the data well, whereas adding more free parameters would result in over-fitting. For details, see SI Section S3 and Figures S6-S7.

We studied eleven nanowire bundles using the technique described above and found a range of values (see Figure S8 for box plots). The mean value of the intrinsic diffusivity was found to be 0.8 cm^2/s. This is very similar to the value of 1.0 cm^2/s for bulk CsPbBr$_3$,[33] and indicates that weak confinement does not affect the excitons' ability to diffuse. This is similar to the findings of Tian et al., who measured carrier diffusion in large, hundred-nm scale nanowires and nanoplatelets of methylammonium lead halide perovskites. They found heterogeneity between samples, but that there is no clear correlation between diffusivity and shape.[37] Our work extends these findings into the quantum confined regime. We also measure a transverse diffusivity of 0.2 cm^2/s, which indicates weak but non-zero inter-nanowire coupling. As energy most likely transfers between nanowires through dipole-dipole coupling, resulting in Förster energy transfer between the nanowires, this value should depend on inter-nanowire separation, and may be tunable by adjusting the ligands. Finally, we extract linear trap densities that range from one trap every 1 μm to one trap every 10 μm (10^{15}-10^{16} cm^{-3}). Though we cannot determine a precise distribution of nanowire lengths, TEM images indicate that they are usually several microns long, suggesting that the number of traps per nanowire is close to 1. Traps could be localized at the ends of the nanowires. Our measured trap densities are slightly higher than those found via electrical transport measurements.[26] This could mean that the pump laser has induced damage, though even with this damage the trap density is notably low.

The CsPbBr$_3$ nanowires were also found to display anisotropic optical properties. This was observed by measuring both the linear absorption and transient absorption of individual bundles with polarized light. Figure 3a shows the absorption spectrum of an individual bundle of 10 nm nanowires at several different optical polarizations. For light polarized along the longitudinal (long) axis of the nanowires (0°), the spectrum is shifted towards lower energies. As the polarization is rotated towards the transverse (short) axis of the nanowires, the spectrum shifts higher in energy. To quantify this shift in absorption onset, we record the half-maximum position of the absorption spectrum and plot it as a function of optical polarization in Figure 3b (orange points). Rotating the optical polarization from being parallel to perpendicular to the bundle shifts the absorption onset by 5 meV. Several bundles were studied, and all showed similar results. In order to verify that this finding is not an artifact of the imaging system, we performed the same measurement on a single large nanowire, about 200 nm in width and 20 µm long. This object has roughly the same dimensions as a bundle, but it is not in the quantum confined regime. We find that the absorption onset, plotted in Figure 3b (black points), is lower in energy (matching bulk CsPbBr$_3$) and is isotropic (see Figure S9 for an image of the nanowire and plots of the absorption spectra). We conclude that in CsPbBr$_3$ nanowires, longitudinally polarized light excites states that are lower in energy than those excited by transverse polarized light. As detailed through the transient absorption measurements below, we attribute this effect to splitting of the band-edge exciton due to the long-range exchange interaction.

Before describing polarization-resolved transient absorption microscopy (TAM) on nanowire bundles, we first establish that the ultrafast dynamics of CsPbBr$_3$ nanowire bundles are similar to those of other lead halide perovskites. Transient absorption (TA) spectra of 10 nm nanowire bundles in solution are shown as a pseudo-color plot in Figure 3c. We also studied un-bundled nanowires (Figure S10), and found nearly identical results, although bundling induces a slight red-shift (not unexpected, given the weak inter-nanowire coupling deduced with stroboSCAT). We observe a prominent ground state bleach (GSB) with a low-energy tail and a photo-induced absorption (PIA) at higher energies. To better visualize the spectra we used Glotaran[38] to fit the data to a four-stage sequential kinetic model: $A_1(\lambda) \xrightarrow{k_1} A_2(\lambda) \xrightarrow{k_2} A_3(\lambda) \xrightarrow{k_3} A_4(\lambda)$, where $A_i(\lambda)$ are the evolution associated spectra (EAS), shown in Figure S11, and k_i is the rate constant for spectrum $A_i(\lambda)$ to evolve into $A_{i+1}(\lambda)$. The fourth EAS has a lifetime much longer than the experimental timescale of 1 ns. We see that the initial spectrum has a high-energy tail and a sub-bandgap PIA feature. Both features are likely due to an initial hot carrier population, which bleaches above-gap transitions, and also causes bandgap renormalization, allowing for sub-bandgap absorption.[39] Both features disappear over the cooling timescale, $1/k_1 = 600\,\mathrm{fs}$, which becomes slower for higher pump fluence (as expected for hot carrier cooling).[36,40] After the initial hot carrier cooling, the subsequent

decay of the GSB can be fit to two exponentials, largely because of biexciton recombination ascertained by plotting $1/\Delta OD$ vs. delay time at the GSB wavelengths at multiple pump fluences (Figure S12). In the case of pure second order decay, this presents as a straight line.[41] We observe a straight line for roughly the first 150 ps, after which it deviates, likely because linear decay channels have become dominant.

There are two other notable features of the TA spectra. The first is the above-gap PIA, which is initially broad and sharpens with time. This has been observed before,[40] but as far as we know its spectral evolution has not been explained. The second is the broad sub-gap negative ΔOD signal. This has also been seen in methylammonium lead bromide, and was attributed to optical phonon-assisted sub-gab absorption.[42] We come to the same conclusion, after ruling out two possible alternatives. One alternative possibility would be that there is decreased scattering in the excited state, but the negative contrast signal in our stroboSCAT measurements indicates that excitons in $CsPbBr_3$ make the material more polarizable, not less. Another possibility would be that the probe induces two-photon absorption, but we varied the probe fluence and found no change in the spectral shape.

Having concluded that $CsPbBr_3$ nanowires display dynamics similar to those of other lead halide perovskites, and that bundling does not impact the dynamics, we turn to polarization-resolved studies of individual bundles with TAM. The setup is similar to one described previously,[43] except that broadband detection has also been implemented rather than employing a single-color probe. In previous work, the ability to measure the probe polarization- and spatially-dependent dynamics of anisotropic samples has revealed key details that are not visible in ensemble measurements. Here we study ten different bundles and find that the TA dynamics are all similar, indicating that the bundles are homogeneous in structure and composition. However, we do find that rotating the probe polarization shifts the TA spectrum. Several normalized and offset TA spectra are shown in Figure 3d, for probe polarization parallel (pink) and perpendicular (blue) to the long axis of a nanowire bundle. They reveal a consistent shift of the GSB feature, which is higher in energy for perpendicular polarization than it is for parallel polarization. Examining the GSB peak for the selected time delays shown in Figure 3d, the magnitude of the shift decreases from 10 meV at early delay times to 5 meV at later delay times, with an uncertainty of less than 1 meV. This is similar in magnitude to the shift seen in the linear absorption spectrum, which was 5 meV (Figure 3a,b), and suggests that the entire exciton spectrum near the band edge experiences polarization-dependent splitting – those states with optical transition dipole moments (TDMs) along the short axis of the nanowire are slightly higher in energy than those with TDMs along the long axis of the nanowire.

We attempted to repeat all optical experiments with bundles of 3 nm nanowires as well in order to investigate the effect of slightly stronger transverse confinement, but these species are much more fragile than 10 nm

nanowires and degrade quickly under pulsed laser excitation. Although it is therefore not possible to quantitate the size of any polarization-dependent shift in the spectral properties of nanowires with widths smaller than 10 nm at this time, we hypothesize that there would be a shift similar to or potentially even larger than what we observe for the 10 nm nanowires.

A shift of any sort must be explained and would be expected if the crystal structure possessed uniaxial/tetragonal or approximately tetragonal symmetry: Indeed our observation that the higher energy transition is polarized preferentially perpendicular to the nanowire axis is consistent with previous measurements in tetragonal $CsPbBr_3$ nanocrystals, where a fine structure splitting of ~1 meV was observed in between the exciton fine structure levels with angular momentum projection ±1 and 0 taken along the *c*-axis, with the ±1 levels, polarized perpendicular to the *c*-axis, being higher in energy, and the 0 level polarized parallel to it.[30] This could imply that nanowires adopt a lower symmetry unit cell with a symmetry axis oriented parallel to the nanowire, leading to anisotropic optical transitions associated with the different fine structure levels. Confirming this hypothesis is complicated by the fact that directly measuring the crystal structure is difficult and the growth direction may be different for nanowires of different sizes.[28] Electronic structure calculations of $CsPbBr_3$ nanowires for various unit cells and orientations would provide valuable insight into the origin of the observed anisotropic transition.

Finally, we performed polarized PL measurements of the 10 nm nanowires in solution. As diagrammed in Figure 4a, the excitation laser at 465 nm was rotated to be polarized either vertically (V) or horizontally (H) in the lab frame. Emission was collected in a direction perpendicular to the excitation beam, with an emission polarizer rotated both vertically and horizontally, generating all possible combinations of the two orthogonal excitation and two orthogonal emission polarizations. Spectra collected in these four configurations are shown in Figure 4b, where the first letter of the legend indicates excitation polarization and the second letter indicates emission polarization. Anisotropy is evident, as the four curves are not identical, but this is not necessarily surprising. In a nanowire geometry classical electrodynamics dictates that both absorption and emission occur preferentially along the long axis, even if the TDM strength is isotropic.[44,45] This is quantified by defining the anisotropy as

$$A = \frac{I_{VV} - I_{VH}}{I_{VV} + I_{VH}} \qquad (3)$$

where the magnitude of A depends on the dielectric constants of the nanowire[46] and the surroundings (see Section S6 for details). Classical electrodynamics predicts $A = 0.09$, but we observe a value of 0.14, an increase of approximately 50%. (This discrepancy also occurs for 408 nm excitation; see Figure S13.) Furthermore, if the optical transitions were isotropic we would expect the three intensities I_{VH}, I_{HV}, and I_{HH} to be identical, and that is not the case. We conclude

11

that the absorption and emission TDMs are themselves anisotropic, possibly due to crystalline asymmetry, and also that the 10 nm nanowires are anisotropically oriented in solution although we cannot calculate the magnitude of the TDM anisotropy without knowing more about the orientational distribution of the nanowires (see Section S6 for details).

We have found several examples of anisotropic behavior in $CsPbBr_3$ nanowires, all of which can be plausibly attributed to geometry or to an asymmetric crystal structure, as opposed to quantum confinement. Exciton transport appears to be driven by geometry, with the lack of inter-nanowire coupling forcing excitons to diffuse primarily along the long axis of the nanowire bundles. The magnitude of the diffusivity, which is comparable to that seen in bulk $CsPbBr_3$, implies that transport is not intrinsically affected by weak confinement. We also observe polarization dependent splitting at the band edge, with transverse polarized light coupling to a manifold of states about 5-10 meV higher in energy than those coupled to by longitudinally polarized light. This is qualitatively consistent with previous measurements in 8-10 nm sized nominally tetragonal $CsPbBr_3$ nanocrystals, where a fine structure splitting of ~1 meV was observed between the exciton fine structure levels with angular momentum projection ±1 and 0 taken along the along the c-axis, with the ±1 levels being higher in energy.[30,31] The interpretation originally given in Refs. 30,31 for the exciton fine structure level ordering in $CsPbBr_3$ nanocrystals was based on the assumption of cubic nanocrystal shape in conjunction with a negative intrinsic tetragonal crystal field splitting and the electron-hole exchange interaction.[23,30,31] However, calculations using density functional theory show that the crystal field in tetragonal $CsPbBr_3$ is positive,[23,47] leading to a level order inconsistent with the experimentally observed fine structure. An alternative explanation for the observed fine structure, proposed in Ref. 24, is connected with the effect of shape anisotropy via the long-range exchange interaction. In fact, $CsPbBr_3$ nanocrystals in the size range reported in Refs. 30,31 have been shown to be elongated along the crystallographic c-axis by 20%.[48] Following Nestoklon et al.,[24] we find that long-range exchange acts in conjunction with the anisotropic shape to create a splitting between the exciton sub-levels with the exciton whose TDM is parallel to the axis of elongation having lower energy than the exciton sublevels whose TDMs are parallel to the short axis.[23,24]

To explore this effect for nanowires, we modelled the nanowire as a rectangular prism with equal x and y (transverse) dimensions, L, but with an unequal z dimension, L_z. We find that the exciton with transition dipole parallel to the axis of elongation (z) has lower energy than the exciton sublevel whose transitions dipoles are parallel to the short axes.[31] The resulting energies are plotted versus the ratio, L_z/L, over the range between the z-dimension of the NW, L_z, and the transverse dimension, L, of the nanowire in Figure S14. Inspection of the plot shows that for large aspect ratios, $L_z/L \gg 1$, the splitting between the z exciton and the transverse excitons approaches $\hbar\omega_i/2$, where $\hbar\omega_i$ is the bulk longitudinal-transverse (LT) splitting, with the z-polarized exciton

12

being lowest in energy, qualitatively consistent with the observed splitting obtained from our nanowire measurements. The value of the LT splitting in bulk CsPbBr$_3$ has recently been measured in CsPbBr$_3$[49] as $\hbar\omega_{\unicode{x13F}} = 5.4$ meV.[50] The larger splitting observed here is likely due in part to dielectric effects as well as possible enhancement of the exciton binding energy or enhanced quantum confinement effects in the nanowires relative to bulk or in nanocrystals, as discussed in the Supporting Information.

The shape asymmetry of the nanowire could also cause the absorption or emission TDMs to be stronger for light polarized along certain nanowire axes, which is what we infer from polarized fluorescence measurements in solution. Unfortunately, because a solution sample comprises many nanowires with different orientations, it is difficult to determine the strength or frequency-dependence of the TDM anisotropy. Studies of CdSe nanoplatelets find that band-edge emission is anisotropic while absorption high above the band edge is isotropic.[51] That could occur in CsPbBr$_3$ as well for high excitation frequency, but the fact that the strength of the anisotropy differs for 465 nm and 408 nm excitation (comparing Figure 4 to Figure S16) implies that neither of these wavelengths are in an isotropic absorption regime. In order to better understand the band-edge structure, polarization-resolved PL measurements of single bundles could be performed at low temperature, which would produce sharper emission peaks[52] and remove the confounding effect of nanowire bundle orientation.[53] Such measurements should be supplemented with electronic structure calculations[54] of CsPbBr$_3$ nanowires with various crystal structures and growth directions, similar to calculations that have been done for near-cubic nanostructures.[55]

Conclusion

We have used several techniques to investigate anisotropic behavior in CsPbBr$_3$ nanowires: stroboSCAT to track exciton diffusion, TA to measure the ultrafast dynamics, local absorption microscopy to measure the polarization-resolved optical coupling to the ground state, TA microscopy to measure the polarization-resolved optical coupling to excited states, and polarized fluorescence to interrogate TDM anisotropy. We observe rapid exciton diffusion along the nanowires' long axis, weak inter-nanowire coupling, and what we take to be an extremely low trap density. Combined with the TA measurements, we see CsPbBr$_3$ nanowires as potential active materials for concentrated photovoltaic applications, in which large exciton densities must be sustained and rapidly transported to an interface for exciton dissociation. From TA we also learn that bundling does not impact nanowire dynamics. The ability to retain their unique character in a complex environment makes CsPbBr$_3$ nanowires a potential building block of tunable electronics that combine several nanostructures to produce novel behaviors.[56]

We have also made several measurements pertinent to the band-edge electronic structure of $CsPbBr_3$ nanowires. Using local absorption and TAM we found that the nanowires display anisotropic optical coupling – the band-edge transition is slightly lower for light polarized along the long nanowire axis than it is for light polarized along the short nanowire axes. Furthermore, polarized fluorescence indicates that the strength of the transition dipole moments is anisotropic as well. These results are qualitatively consistent with splitting of the band-edge exciton due to the long-range exchange interaction in conjunction with the shape anisotropy of the nanowire. The measured splitting is larger than would be expected using bulk exciton parameters, which suggests that enhancement of the exciton binding energy due the 1D effects and dielectric confinement play a role in the splitting. Polarization-resolved PL measurements of single nanowire bundles at low temperature could in the future resolve some of the questions raised herein.
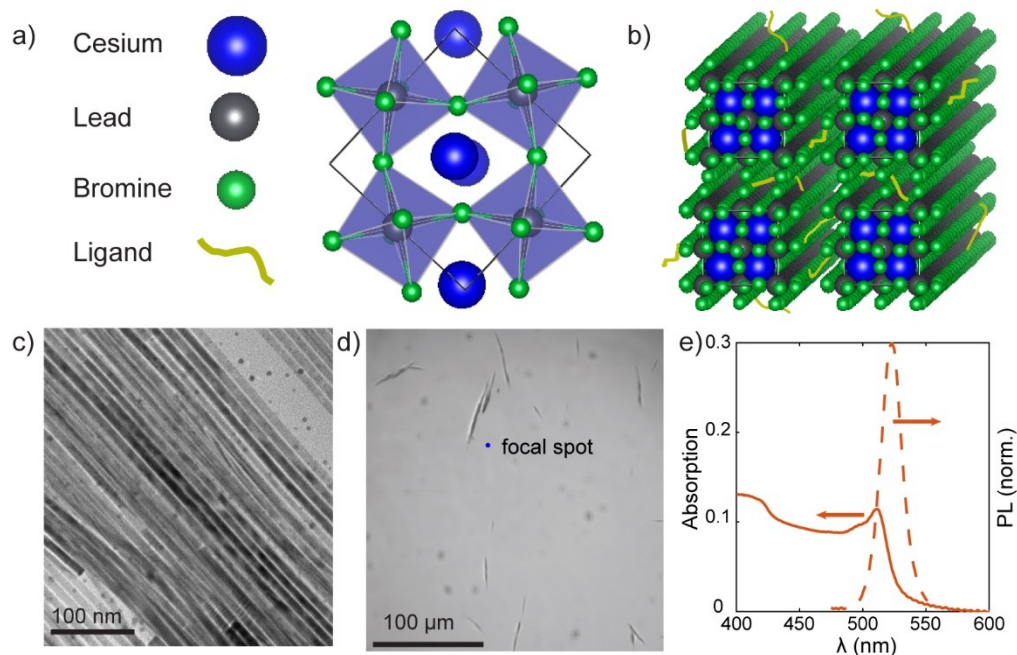
Acknowledgements

Figure 1: Structure and properties of CsPbBr$_3$ nanowire bundles. (a) Unit cell of orthorhombic CsPbBr$_3$ and (b) Cartoon nanowire bundle. To visualize the nanowire, many fewer ligands are depicted than are actually present.(c) TEM image of 10 nm diameter nanowire bundles, showing alignment and monodispersity of nanowires. (d) Optical image of 10 nm diameter nanowire bundles, showing their size compared to a typical pump laser focal spot used in transient absorption microscopy (blue dot). (e) Absorption (solid lines) and photoluminescence (dashed lines) of 10 nm nanowires.
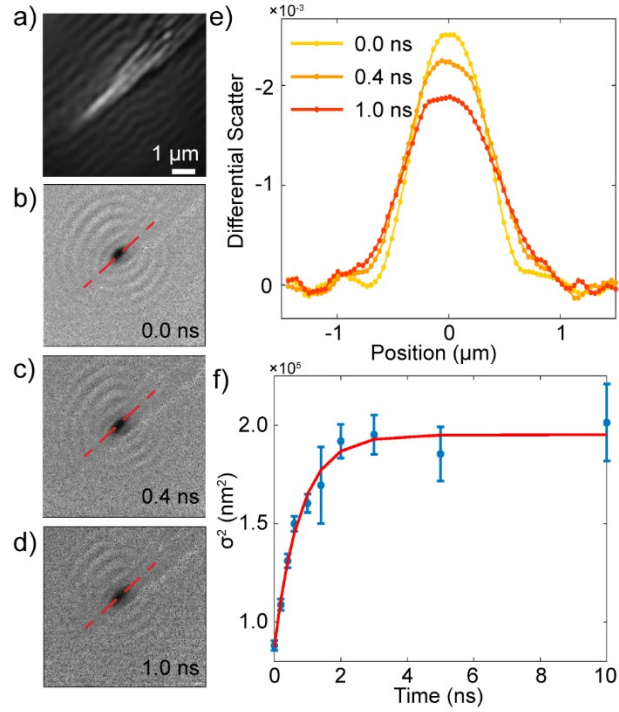
Figure 2: Observing diffusion of energy through nanowires with stroboSCAT. (a) Interferometric scattering image of 10 nm diameter nanowire bundle. (b)-(d) Differential scattering images at time delays of 0.0 ns, 0.4 ns, and 1.0 ns after pump excitation, showing longitudinal diffusion. (e) Profiles along the paths indicated by red lines in (b)-(d), showing diffusion. (f) Mean squared displacement of the Gaussian fits to scattering profiles such as those shown in (e). The data are fit to an exponentially decaying diffusivity (red line).
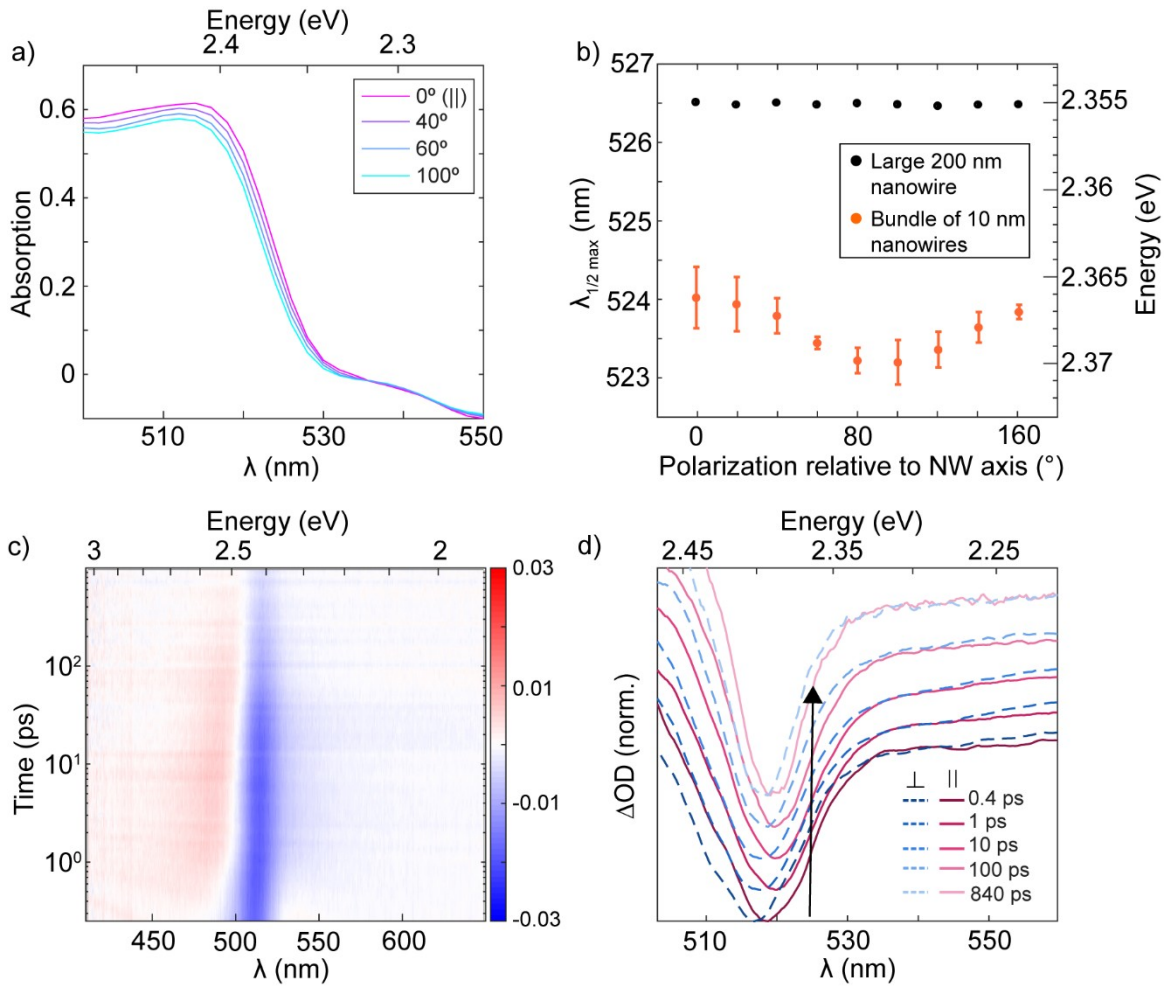
Figure 3: Polarization resolved optical measurements of 10 nm diameter CsPbBr₃ nanowire bundles. (a) Local linear absorption spectra of a single bundle for several polarizations. (b) Absorption onset vs. polarization (orange) showing oscillatory dependence. The polarization-resolved absorption onset for a large, 200 nm nanowire (black) shows no oscillation and is red shifted. (c) Transient Absorption (TA) map for 10 nm nanowire bundles in solution, and (d) normalized TA spectra at selected times for a single bundle with probe polarized along the longitudinal (pink) and transverse (blue) direction, showing a persistent shift of about 5-10 meV. The spectra are offset by delay time, for clarity, and the arrow is meant to guide the eye from the early-time spectra, on the bottom, to the later-time spectra, on the top.
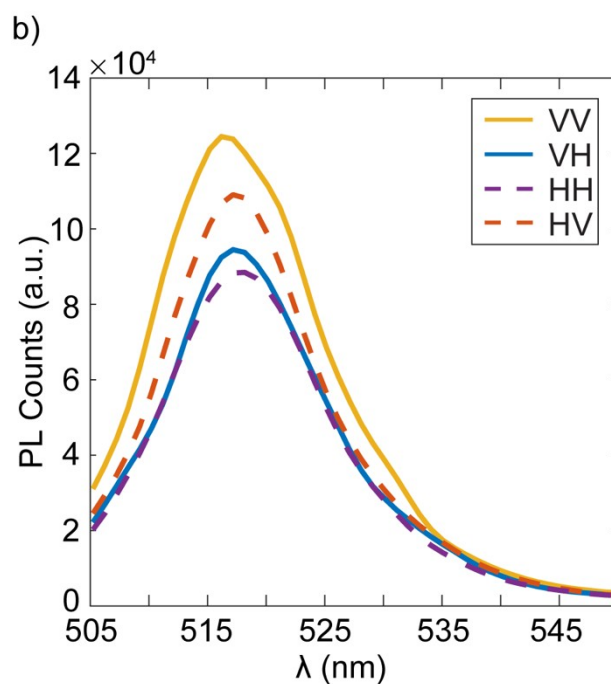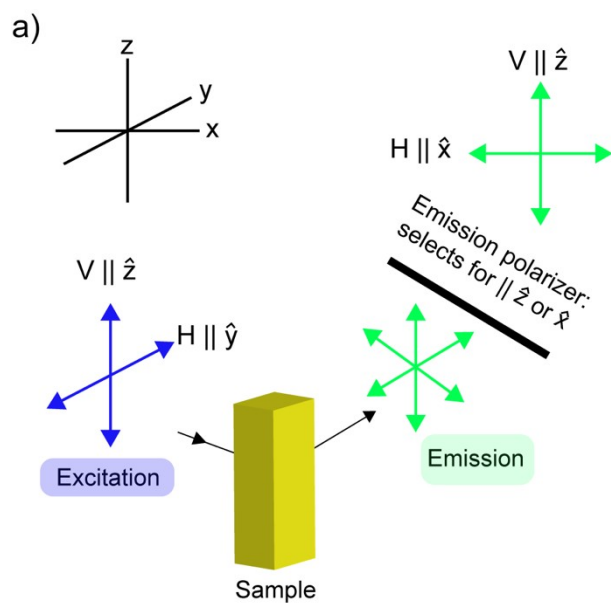
Figure 4: Polarization-dependent PL (a) schematic and (b) spectra of 10 nm diameter CsPbBr$_3$ nanowires in cyclohexane, excited at 465 nm. The first letter of the legend indicates the polarization of the excitation beam (vertical or horizontal) and the second letter indicates the polarization of the measured emission.
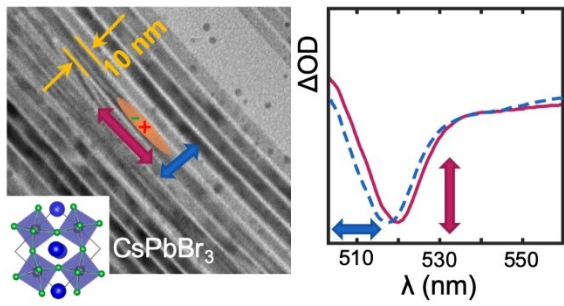
(1) Zhang, J.; Bai, D.; Jin, Z.; Bian, H.; Wang, K.; Sun, J.; Wang, Q.; Liu, S. F. 3D-2D-0D Interface Profiling for Record Efficiency All-Inorganic CsPbBrI 2 Perovskite Solar Cells with Superior Stability. *Adv. Energy Mater.* **2018**, *1703246*, 1703246. https://doi.org/10.1002/aenm.201703246.

(2) Chen, H.; Xiang, S.; Li, W.; Liu, H.; Zhu, L.; Yang, S. Inorganic Perovskite Solar Cells: A Rapidly Growing Field. *Sol. RRL* **2018**, *6*, 1700188. https://doi.org/10.1002/solr.201700188.

(3) Eaton, S. W.; Lai, M.; Gibson, N. A.; Wong, A. B.; Dou, L.; Ma, J.; Wang, L.-W.; Leone, S. R.; Yang, P. Lasing in Robust Cesium Lead Halide Perovskite Nanowires. *Proc. Natl. Acad. Sci.* **2016**, *113* (8), 1993. https://doi.org/10.1073/pnas.1600789113.

(4) Fu, Y.; Zhu, H.; Stoumpos, C. C.; Ding, Q.; Wang, J.; Kanatzidis, M. G.; Zhu, X.; Jin, S. Broad Wavelength Tunable Robust Lasing from Single-Crystal Nanowires of Cesium Lead Halide Perovskites (CsPbX3, X = Cl, Br, I). *ACS Nano* **2016**, *10* (8), 7963–7972. https://doi.org/10.1021/acsnano.6b03916.

(5) Zhang, Y.; Liu, J.; Wang, Z.; Xue, Y.; Ou, Q.; Polavarapu, L.; Zheng, J.; Qi, X.; Bao, Q. Synthesis, Properties, and Optical Applications of Low-Dimensional Perovskites. *Chem. Commun.* **2016**, *52* (94), 13637–13655. https://doi.org/10.1039/c6cc06425f.

(6) Zhou, Y.; Luo, J.; Zhao, Y.; Ge, C.; Wang, C.; Gao, L.; Zhang, C.; Hu, M.; Niu, G.; Tang, J. Flexible Linearly Polarized Photodetectors Based on All-Inorganic Perovskite CsPbI 3 Nanowires. *Adv. Opt. Mater.* **2018**, *1800679*, 1800679. https://doi.org/10.1002/adom.201800679.

(7) Chen, Q.; Wu, J.; Ou, X.; Huang, B.; Almutlaq, J.; Zhumekenov, A. A.; Guan, X.; Han, S.; Liang, L.; Yi, Z.; et al. All-Inorganic Perovskite Nanocrystal Scintillators. *Nature* **2018**, *561*, 88–93. https://doi.org/10.1038/s41586-018-0451-1.

(8) Wang, Y.; Li, X.; Song, J.; Xiao, L.; Zeng, H.; Sun, H. All-Inorganic Colloidal Perovskite Quantum Dots: A New Class of Lasing Materials with Favorable Characteristics. *Adv. Mater.* **2015**, *27* (44), 7101–7108. https://doi.org/10.1002/adma.201503573.

(9) Raja, S. N.; Bekenstein, Y.; Koc, M. A.; Fischer, S.; Zhang, D.; Lin, L.; Ritchie, R. O.; Yang, P.; Alivisatos, P. Encapsulation of Perovskite Nanocrystals into Macroscale Polymer Matrices: Enhanced Stability and Polarization. *ACS Appl. Mater. Interfaces* **2016**, *8*, acsami.6b09443. https://doi.org/10.1021/acsami.6b09443.

(10) Becker, M. A.; Vaxenburg, R.; Nedelcu, G.; Sercel, P. C.; Shabaev, A.; Mehl, M. J.; Michopoulos, J. G.; Lambrakos, S. G.; Bernstein, N.; Lyons, J. L.; et al. Bright Triplet Excitons in Caesium Lead Halide Perovskites. *Nature* **2018**, *553* (7687), 189–193. https://doi.org/10.1038/nature25147.

(11) Zhang, D.; Yu, Y.; Bekenstein, Y.; Wong, A. B.; Alivisatos, A. P.; Yang, P. Ultrathin Colloidal Cesium Lead Halide Perovskite Nanowires. *J. Am. Chem. Soc.* **2016**, jacs.6b08373. https://doi.org/10.1021/jacs.6b08373.

(12) Bekenstein, Y.; Koscher, B. A.; Eaton, S. W.; Yang, P.; Alivisatos, A. P. Highly Luminescent Colloidal Nanoplates of Perovskite Cesium Lead Halide and Their Oriented Assemblies. *J. Am. Chem. Soc.* **2015**, *137* (51), 16008–16011. https://doi.org/10.1021/jacs.5b11199.

(13) Ravi, V. K.; Swarnkar, A.; Chakraborty, R.; Nag, A. Excellent Green but Less Impressive Blue Luminescence from CsPbBr3 Perovskite Nanocubes and Nanoplatelets. *Nanotechnology* **2016**, *27* (32). https://doi.org/10.1088/0957-4484/27/32/325708.

(14) Yarita, N.; Tahara, H.; Ihara, T.; Kawawaki, T.; Sato, R.; Saruyama, M.; Teranishi, T.; Kanemitsu, Y. Dynamics of Charged Excitons and Biexcitons in CsPbBr3Perovskite Nanocrystals Revealed by Femtosecond Transient-Absorption and Single-Dot Luminescence Spectroscopy. *J. Phys. Chem. Lett.* **2017**, *8* (7), 1413–1418. https://doi.org/10.1021/acs.jpclett.7b00326.

(15) Castaneda, J. A.; Nagamine, G.; Yassitepe, E.; Bonato, L. G.; Voznyy, O.; Hoogland, S.; Nogueira, A. F.; Sargent, E. H.; Cruz, C. H. B.; Padilha, L. A. Efficient Biexciton Interaction in Perovskite Quantum Dots Under Weak and Strong Confinement. *ACS Nano* **2016**, *10*, 8603–8609. https://doi.org/10.1021/acsnano.6b03908.

(16) Gibson, N. A.; Koscher, B. A.; Alivisatos, A. P.; Leone, S. R. Excitation Intensity Dependence of Photoluminescence Blinking in CsPbBr 3 Perovskite Nanocrystals. *J. Phys. Chem. C* **2018**, *122* (22), 12106–12113. https://doi.org/10.1021/acs.jpcc.8b03206.

(17) Di Stasio, F.; Imran, M.; Akkerman, Q. A.; Prato, M.; Manna, L.; Krahne, R. Reversible Concentration-Dependent Photoluminescence Quenching and Change of Emission Color in CsPbBr3Nanowires and Nanoplatelets. *J. Phys. Chem. Lett.* **2017**, *8* (12), 2725–2729. https://doi.org/10.1021/acs.jpclett.7b01305.

(18) Zhu, Q.; Karlsson, K. F.; Pelucchi, E.; Kapon, E. Transition from Two-Dimensional to Three-Dimensional Quantum Confinement in Semiconductor Quantum Wires/Quantum Dots. *Nano Lett.* **2007**, *7* (8), 2227–2233. https://doi.org/10.1021/nl0706650.

(19) Htoon, H.; Hollingsworth, J. A.; Dickerson, R.; Klimov, V. I. Effect of Zero- to One-Dimensional Transformation on Multiparticle Auger Recombination in Semiconductor Quantum Rods. *Phys. Rev. Lett.* **2003**, *91* (22), 1–4. https://doi.org/10.1103/PhysRevLett.91.227401.

(20) Blancon, J. C.; Tsai, H.; Nie, W.; Stoumpos, C. C.; Pedesseau, L.; Katan, C.; Kepenekian, M.; Soe, C. M. M.; Appavoo, K.; Sfeir, M. Y.; et al. Extremely Efficient Internal Exciton Dissociation through Edge States in Layered 2D Perovskites. *Science* **2017**, *355* (6331), 1288–1292. https://doi.org/10.1126/science.aal4211.

(21) Sercel, P.; Vahala, K. Polarization Dependence of Optical Absorption and Emission in Quantum Wires. *Phys. Rev. B* **1991**, *44* (11), 5681–5691. https://doi.org/10.1103/PhysRevB.44.5681.

(22) Delor, M.; Weaver, H. L.; Yu, Q.; Ginsberg, N. S. Three-Dimensional Imaging of Material Functionality through Nanoscale Tracking of Energy Flow. *Nat. Mater.* **2019**. https://doi.org/10.1038/s41563-019-0498-x.

(23) Sercel, P. C.; Lyons, J. L.; Wickramaratne, D.; Vaxenburg, R.; Bernstein, N.; Efros, A. L. Exciton Fine Structure in Perovskite Nanocrystals. *Nano Lett.* **2019**, *19*, 4068–4077. https://doi.org/10.1021/acs.nanolett.9b01467.

(24) Nestoklon, M. O.; Goupalov, S. V.; Dzhioev, R. I.; Ken, O. S.; Korenev, V. L.; Kusrayev, Y. G.; Sapega, V. F.; De Weerd, C.; Gomez, L.; Gregorkiewicz, T.; et al. Optical Orientation and Alignment of Excitons in Ensembles of Inorganic Perovskite Nanocrystals. *Phys. Rev. B* **2018**, *97* (23), 1–10. https://doi.org/10.1103/PhysRevB.97.235304.

(25) Shabaev, A.; Efros, A. L. 1D Exciton Spectroscopy of Semiconductor Nanorods. *Nano Lett.* **2004**, *4* (10), 1821–1825. https://doi.org/10.1021/nl049216f.

(26) Zhang, D.; Yang, Y.; Bekenstein, Y.; Yu, Y.; Gibson, N. A.; Wong, A. B.; Eaton, S. W.; Kornienko, N.; Kong, Q.; Lai, M.; et al. Synthesis of Composition Tunable and Highly Luminescent Cesium Lead Halide Nanowires through Anion-Exchange Reactions. *J. Am. Chem. Soc.* **2016**, *138* (23), 7236–7239. https://doi.org/10.1021/jacs.6b03134.

(27) Zhang, D.; Eaton, S. W.; Yu, Y.; Dou, L.; Yang, P. Solution-Phase Synthesis of Cesium Lead Halide Perovskite Nanowires. *J. Am. Chem. Soc.* **2015**, *137* (29), 9230–9233. https://doi.org/10.1021/jacs.5b05404.

(28) Imran, M.; Di Stasio, F.; Dang, Z.; Canale, C.; Khan, A. H.; Shamsi, J.; Brescia, R.; Prato, M.; Manna, L. Colloidal Synthesis of Strongly Fluorescent CsPbBr3Nanowires with Width Tunable down to the Quantum Confinement Regime. *Chem. Mater.* **2016**, *28* (18), 6450–6454. https://doi.org/10.1021/acs.chemmater.6b03081.

(29) Ten Brinck, S.; Infante, I. Surface Termination, Morphology, and Bright Photoluminescence of Cesium Lead Halide Perovskite Nanocrystals. *ACS Energy Lett.* **2016**, *1* (6), 1266–1272. https://doi.org/10.1021/acsenergylett.6b00595.

(30) Fu, M.; Tamarat, P.; Huang, H.; Even, J.; Rogach, A. L.; Lounis, B. Neutral and Charged Exciton Fine Structure in Single Lead Halide Perovskite Nanocrystals Revealed by Magneto-Optical Spectroscopy. *Nano Lett.* **2017**, *17* (5), 2895–2901. https://doi.org/10.1021/acs.nanolett.7b00064.

(31) Ramade, J.; Andriambariarijaona, L. M.; Steinmetz, V.; Goubet, N.; Legrand, L.; Barisien, T.; Bernardot, F.; Testelin, C.; Lhuillier, E.; Bramati, A.; et al. Fine Structure of Excitons and Electron-Hole Exchange Energy in Polymorphic CsPbBr3single Nanocrystals. *Nanoscale* **2018**, *10* (14), 6393–6401. https://doi.org/10.1039/c7nr09334a.

(32) Protesescu, L.; Yakunin, S.; Bodnarchuk, M. I.; Krieg, F.; Caputo, R.; Hendon, C. H.; Yang, R. X.; Walsh, A.; Kovalenko, M. V. Nanocrystals of Cesium Lead Halide Perovskites (CsPbX\textlessinf\textgreater3\textless/Inf\textgreater, X = Cl, Br, and I): Novel Optoelectronic Materials Showing Bright Emission with Wide Color Gamut. *Nano Lett.* **2015**, *15* (6), 3692–3696. https://doi.org/10.1021/nl5048779.

(33) Delor, M.; Weaver, H. L.; Yu, Q.; Ginsberg, N. S. Universal Imaging of Material Functionality through Nanoscale Tracking of Energy Flow. *ArXiv*. https://doi.org/1805/1805.09982.

(34) Penwell, S. B.; Ginsberg, L. D. S.; Noriega, R.; Ginsberg, N. S. Resolving Ultrafast Exciton Migration in Organic Solids at the Nanoscale. *Nat. Mater.* **2017**, *16* (11), 1136–1141. https://doi.org/10.1038/NMAT4975.

(35) Guo, Z.; Wan, Y.; Yang, M.; Snaider, J.; Zhu, K.; Huang, L. Long-Range Hot-Carrier Transport in Hybrid Perovskites Visualized by Ultrafast Microscopy. *Science* **2017**, *356* (6333), 59–62. https://doi.org/10.1126/science.aam7744.

(36) Fu, J.; Xu, Q.; Han, G.; Wu, B.; Huan, C. H. A.; Leek, M. L.; Sum, T. C. Hot Carrier Cooling Mechanisms in Halide Perovskites. *Nat. Commun.* **2017**, *8* (1). https://doi.org/10.1038/s41467-017-01360-3.

(37) Tian, W.; Zhao, C.; Leng, J.; Cui, R.; Jin, S. Visualizing Carrier Diffusion in Individual Single-Crystal Organolead Halide Perovskite Nanowires and Nanoplates. *J. Am. Chem. Soc.* **2015**, *137* (39), 12458–12461. https://doi.org/10.1021/jacs.5b08045.

(38) Snellenburg, J. J.; Laptenok, S. P.; Seger, R.; Mullen, K. M.; van Stokkum, I. H. M. Glotaran : A Java -Based Graphical User Interface for the R Package TIMP. *J. Stat. Softw.* **2012**, *49* (3). https://doi.org/10.18637/jss.v049.i03.

(39) Price, M. B.; Butkus, J.; Jellicoe, T. C.; Sadhanala, A.; Briane, A.; Halpert, J. E.; Broch, K.; Hodgkiss, J. M.; Friend, R. H.; Deschler, F. Hot-Carrier Cooling and Photoinduced Refractive Index Changes in Organic-Inorganic Lead Halide Perovskites. *Nat. Commun.* **2015**, *6* (May), 1–8. https://doi.org/10.1038/ncomms9420.

(40) Mondal, N.; Samanta, A. Complete Ultrafast Charge Carrier Dynamics in Photo-Excited All-Inorganic Perovskite Nanocrystals (CsPbX3). *Nanoscale* **2017**, *9*, 1878–1885. https://doi.org/10.1039/c6nr09422h.

(41) Manser, J. S.; Kamat, P. V. Band Filling with Free Charge Carriers in Organometal Halide Perovskites. *Nat Photonics* **2014**, *8* (9), Ahead of Print. https://doi.org/10.1038/nphoton.2014.171.

(42) Telfah, H.; Jamhawi, A.; Teunis, M. B.; Sardar, R.; Liu, J. Ultrafast Exciton Dynamics in Shape-Controlled Methylammonium Lead Bromide Perovskite Nanostructures: Effect of Quantum Confinement on Charge Carrier Recombination. *J. Phys. Chem. C* **2017**, *121* (51), 28556–28565. https://doi.org/10.1021/acs.jpcc.7b10377.

(43) Folie, B. D.; Haber, J. B.; Refaely-Abramson, S.; Neaton, J. B.; Ginsberg, N. S. Long-Lived Correlated Triplet Pairs in a π-Stacked Crystalline Pentacene Derivative. *J. Am. Chem. Soc.* **2018**, *140* (6), 2326–2335. https://doi.org/10.1021/jacs.7b12662.

(44) Ruda, H. E.; Shik, A. Polarization-Sensitive Optical Phenomena in Semiconducting and Metallic Nanowires. *Phys. Rev. B* **2005**, *72* (11), 115308. https://doi.org/10.1103/PhysRevB.72.115308.

(45) Efros, A. L.; Rosen, M.; Averboukh, B.; Kovalev, D.; Ben-Chorin, M.; Koch, F. Nonlinear Optical Effects in Porous Silicon: Photoluminescence Saturation and Optically Induced Polarization Anisotropy. *Phys. Rev. B - Condens. Matter Mater. Phys.* **1997**, *56* (7), 3875–3884. https://doi.org/10.1103/PhysRevB.56.3875.

(46) Maqbool, M.; Rehman, G.; Ali, L.; Shafiq, M.; Iqbal, R.; Ahmad, R.; Khan, T.; Jalali-Asadabadi, S.; Maqbool, M.; Ahmad, I. Structural, Electronic and Optical Properties of CsPbX3(X=Cl, Br, I) for Energy Storage and Hybrid Solar Cell Applications. *J. Alloys Compd.* **2017**, *705*, 828–839. https://doi.org/10.1016/j.jallcom.2017.02.147.

(47) Sercel, P. C.; Lyons, J. L.; Bernstein, N.; Efros, A. L. Quasi-Cubic Model for Metal Halide Perovskite Nanocrystals. *Submitted*.

(48) Bertolotti, F.; Protesescu, L.; Kovalenko, M. V.; Yakunin, S.; Cervellino, A.; Billinge, S. J. L.; Terban, M. W.; Pedersen, J. S.; Masciocchi, N.; Guagliardi, A. Coherent Nanotwins and Dynamic Disorder in Cesium Lead Halide Perovskite Nanocrystals. *ACS Nano* **2017**, *11* (4), 3819–3831. https://doi.org/10.1021/acsnano.7b00017.

(49) Yang, Z.; Surrente, A.; Galkowski, K.; Miyata, A.; Portugall, O.; Sutton, R. J.; Haghighirad, A. A.; Snaith, H. J.; Maude, D. K.; Plochocka, P.; et al. Impact of the Halide Cage on the Electronic Properties of Fully Inorganic Cesium Lead Halide Perovskites. *ACS Energy Lett.* **2017**, *2* (7), 1621–1627. https://doi.org/10.1021/acsenergylett.7b00416.

(50) Belykh, V. V.; Yakovlev, D. R.; Glazov, M. M.; Grigoryev, P. S.; Hussain, M.; Rautert, J.; Dirin, D. N.; Kovalenko, M. V.; Bayer, M. Coherent Spin Dynamics of

Electrons and Holes in CsPbBr3 Perovskite Crystals. *Nat. Commun.* **2019**, *10* (1). https://doi.org/10.1038/s41467-019-08625-z.

(51) Ma, X.; Diroll, B. T.; Cho, W.; Fedin, I.; Schaller, R. D.; Talapin, D. V.; Wiederrecht, G. P. Anisotropic Photoluminescence from Isotropic Optical Transition Dipoles in Semiconductor Nanoplatelets. *Nano Lett.* **2018**, *18*, 4647–4652. https://doi.org/10.1021/acs.nanolett.8b00347.

(52) Diroll, B. T.; Zhou, H.; Schaller, R. D. Low-Temperature Absorption, Photoluminescence, and Lifetime of CsPbX3 (X = Cl, Br, I) Nanocrystals. *Adv. Funct. Mater.* **2018**, *3*, 1–7. https://doi.org/10.1002/adfm.201800945.

(53) Täuber, D.; Dobrovolsky, A.; Camacho, R.; Scheblykin, I. G. Exploring the Electronic Band Structure of Organometal Halide Perovskite via Photoluminescence Anisotropy of Individual Nanocrystals. *Nano Lett.* **2016**, *16* (8), 5087–5094. https://doi.org/10.1021/acs.nanolett.6b02012.

(54) Berger, R. F. Design Principles for the Atomic and Electronic Structure of Halide Perovskite Photovoltaic Materials: Insights from Computation. *Chem. - Eur. J.* **2018**, *24* (35), 8708–8716. https://doi.org/10.1002/chem.201706126.

(55) Ben Aich, R.; Saïdi, I.; Ben Radhia, S.; Boujdaria, K.; Barisien, T.; Legrand, L.; Bernardot, F.; Chamarro, M.; Testelin, C. Bright-Exciton Splittings in Inorganic Cesium Lead Halide Perovskite Nanocrystals. *Phys. Rev. Appl.* **2019**, *11* (3), 034042. https://doi.org/10.1103/PhysRevApplied.11.034042.

(56) Chen, J.-S.; Doane, T. L.; Li, M.; Zang, H.; Maye, M. M.; Cotlet, M. 0D-2D and 1D-2D Semiconductor Hybrids Composed of All Inorganic Perovskite Nanocrystals and Single-Layer Graphene with Improved Light Harvesting. *Part. Part. Syst. Charact.* **2017**, *1700310*, 1700310. https://doi.org/10.1002/ppsc.201700310.

For Table of Contents Only